Modal decompositions of the local electromagnetic density of states and spatially resolved electron energy loss probability in terms of geometric modes

Guillaume Boudarham and Mathieu Kociak*

Laboratoire de Physique des Solides CNRS/UMR8502, Bâtiment 510, Univ. Paris-Sud, Orsay, 91405, France

(Received 3 November 2011; revised manuscript received 27 April 2012; published 28 June 2012)

We present universal modal decompositions of the quasistatic electromagnetic local density of states (EMLDOS) of nanoparticles in the presence of dissipation and for arbitrary materials. This relies on a generic and universal description of the optical eigenmodes in arbitrary structures. In this description, already developed in various former theories, the eigenmodes are independent of the energy, scale invariant, and depend only on the structures shapes. For these reasons, we call the modes *geometric eigenmodes*. A direct analogy with the well-known modal decomposition of the EMLDOS in the case of nondissipative photonic modes is drawn in the special case of a material described by a Drude's model. Moreover, we show that this formalism is suitable to describe the electron energy loss spectroscopy and some scanning near optical field microscopy experiments. The link between such experiments and the mapping of the geometric mode is analyzed. In particular, this allows us to show that the delocalization of the inelastic signal can be interpreted as a convolution of the surface eigencharges at the boundary of the particle with the Coulombian interaction that arises in both experimental set up. A local density of states for the geometric eigenmodes depending only on the geometry of the particle is introduced, by analogy with the well-known EMLDOS for the photonic eigenmodes. This density of states and the related Green's functions, which have a very simple and concise form, are shown to be capable of generating all relevant quantities in the quasistatic approximation. Finally, we discuss the impact of the energy dispersion of the dielectric functions on the loss of spatial coherence of the geometric eigenmodes.

DOI: 10.1103/PhysRevB.85.245447 PACS number(s): 73.20.Mf, 41.20.Cv, 79.20.Uv, 78.67.−n

I. INTRODUCTION

In the past ten years, there has been dramatic improvements in nanooptics, the science of visible light at the nanometer scale, and the related nanoplasmonics, the science of plasmons in nanoobjects. These improvements rely on the design of nanoobjects with targeted purposes, such as photonic nanowires,[1,2] plasmonic nanoparticles,[3] or semiconductor quantum dots,[4] but also on the development of new types of microscopies and/or spectroscopies with spatial resolutions that are well below the wavelength of light. One can cite the development of the scanning near-field optical microscopies (SNOM) [which exist under many different form,[5] among which the photon scanning tunneling microscope (PSTM)[6]], the cathodoluminescence (CL),[7,8] the electron energy loss spectroscopy (EELS),[3,9,10] the photoelectron emission microscopy (PEEM)[11] among other. It is very interesting to note that most of these techniques, when applied to photonic or plasmonic structures have been shown to be related to the eigenmodes of the structures. More precisely, under circumstance (see Sec. X), the SNOM signal can be related to a very comprehensive and synthetic quantity, namely, the electromagnetic local density of states (EMLDOS).[12] Such a relation has also been extended to the case of plasmonic structures in SNOM and PSTM.[13] and later for EELS and CL.[14] The general form of the EMLDOS is given by the imaginary part of the dyadic Green's tensor from Maxwell's equation. Such a definition is very efficient but acts as a black box. Indeed, one can compute the EMLDOS without getting much insight in the physics below. In the case of photonic structures, and forgetting its magnetic part that is not relevant above the IR region,[13] the EMLDOS has a very intuitive definition:[12,15] for a given eigenenergy (eigenwavelength) at each point of the space and for a given electrical field polarization, it is given by the square modulus of the associated eigenelectrical field along the given polarization. Otherwise speaking, the EMLDOS is the sum over all modes, each defined by a well defined energy, of the square modulus of the electrical eigenfield weighted by a delta function peaked at the eigenenergy. As such, the EMLDOS at a given energy is reflecting the spatial variation of the optical excitation of interest, i.e., the solutions of the Maxwell's equations, just like the electronic local density of states is reflecting the spatial distribution of the Schrödinger's equation. Experimentally, the energy filtered maps recorded through various techniques seem to reproduce well the plasmon wave oscillations.[3] At the same time, the theory is predicting a direct relationship between the EMLDOS or related quantities and the experiments, whatever the nature of the underlying modes (plasmons, photons, polaritons, etc.). Thus it sounds at first sight obvious to extend such an interpretation to plasmonic systems. However, the question to know what is the meaning of the EMLDOS for a dissipative system such as metallic nanoparticles subtending plasmons waves is worth to address. More generally, we can wonder what is the meaning and definition of the eigenstates for such systems, in particular, the counting of modes in the case of dissipation is all but trivial.

These problems were partly addressed already in the past, initially in the context of EELS. Ouyang and Isaacson,[16] first proposed a modal decomposition of the spatially resolved EELS in the nonretarded approximation and in the local continuum dielectric framework with an arbitrary dielectric function for a system consisting of only two types of materials. They showed that the surface eigencharges were solutions of an eigenvalue integral equation derived from the Poisson's equation and where essentially the continuity

conditions at the interface between the materials were totally included. Interestingly, the eigenvalues were not energies nor frequencies. Later, García de Abajo and Aizpurua[17] put the former theory on safe theoretical grounds by developing a robust boundary element method (BEM) theory and numerical tool for an arbitrary number of different materials. One main result was the existence of an integral eigenvalue equation for the eigenmodes, from which the EELS was deduced. Aizpurua *et al*.[20] thus used this theory for describing several geometries probed by EELS (wedges, interfaces, etc.) and interpreting the results in terms of eigenmodes with well defined energies. García de Abajo *et al*. extended the theory for the relativistic case.[21] Due to the intricate nature of the relativistic theory, the eigenmodes were more difficult to grab. In these works,[17,20] it was already noted that, in the case of EELS calculations in the nonretarded approximation, the modes were not depending directly on the energy, but rather on the different dielectric functions. Also, still in the nonretarded approximation, the EELS signal was not depending on any relevant scale but only on the ratio of dimensions. This scale invariance was later originally recognized by Fredkin and Mayergoyz[18] in the general framework of the Poisson's equation solving, i.e., the scale invariance is a property of the eigenmodes in the nonretarded case, not of the EELS theory. Formally, the EELS modal decomposition could thus be done without explicitly describing the energy dependence, and was only dependent on the geometry of the system under consideration and not on the real dimensions or details of the dielectric functions. This was pointed out as an interesting way of formally solving an EELS problem for a given geometry (without the burden of solving the equations at all energies), and then for almost the same computational effort the problem could be solved for arbitrary dielectric functions.[17] Interestingly, the imaginary nature of the dielectric functions did not seem to affect the modal decomposition. Hohenester and Krenn[22] also discussed the same equation, and gave a well defined form (within the Drude's model) for the dielectric function in order to discuss modes in arbitrary shaped structures. They later proposed a partial eigenmodes decomposition for the Green's function associated with the potential.[23] Later, Mayergoyz *et al*. showed that the solution of the above mentioned integral equation could be seen as a biorthogonal basis[24] (the biorthogonality between the surface eigencharges only was already pointed out by Ouyang and Isaacson),[25] composed, namely, of surface eigencharges and surface eigendipoles (pointing perpendicular to the surface). For slightly different reasons, another generic eigenmodes solution of a similar eigenvalue equation derived from the Poisson's equation, but valid for the potential rather than the charge, and where the boundary conditions were not explicitly taken into account has been given by Stockmann *et al*.[19,26] in the nonretarded approximation. In this work, a modal decomposition of the Green's function for the potential was given with an explicit energy dependence, although the fact that the modes were material independent was noted. Thus different views of the same problem have been discussed in the past ten years, but no generic theory emerged yet. In particular, no generic modal decomposition of the EMLDOS has been given, and the link between the different approaches (different eigenvalues equation for the same problem, different Green's functions, different types of eigenfunctions, some being orthogonal when others are not) has not been established. Also, the surprising result that eigenmodes can be defined whatever the underlying dielectric function, especially in the case of dissipative metals or even semiconductors, has not been discussed to the best of our knowledge.

This is this paper's aim to introduce several modal decompositions of the EMLDOS and related experimental quantities (EELS, SNOM) in this scale invariant, energy independent modes (later called *geometric eigenmodes*) basis, and to discuss how scale invariance and energy independence affect the spatial coherence of measured eigenmodes.

The paper is thus organized as follows. We first introduce the well-known equations and expressions leading to a scale invariant, energy independent description of the eigenmodes as surface charges and dipoles in Sec. II. We then deduce various modal decompositions of electromagnetic quantities such as the scalar Green's function in Sec. III or the dyadic Green's tensor in Sec. IV that are needed to introduce the EMLDOS and other quantity modal decompositions. A new quantity, namely, an energy and scale independent Green's function for the eigenmodes is then introduced in Sec. V. Its spectral function exhibits poles in a relevant complex plane that are perfectly defined even in the case of arbitrary complex dielectric functions describing the underlying materials. These poles are identified as *geometric modes*. We establish a link between the geometric Green's function and the more commonly used Green's functions. We then exemplify the use of these modal decompositions for understanding experimental results; in Sec. VI, we derive a modal decomposition for plasmonic structures with dissipation. In Sec. VII, we derive a formal expression of the LDOS for the geometric eigenmodes that does not depend on the energy or on the underlying media. In Secs. IX and X, we derive various equivalent modal decompositions of relevant experimental quantities for EELS and SNOM. Finally, in Sec. XII, we describe in this formalism the loss of spatial coherence of the geometric modes in the presence of dissipative dispersion relations.

Frequency-dependent dielectric functions will be used to describe the electric response of different materials. Atomic units ($\hbar = e = m = 1$) and CGS units for the electromagnetic fields will be used from now, unless otherwise specified.

II. GEOMETRIC EIGENMODES

It is well-known that the calculation, in the nonretarded approximation, of the induced electromagnetic fields due to the interaction between an electric field (from a test charge) and a particle of arbitrary shape, described by the local dielectric function $\epsilon_1(\omega)$ and embedded in an homogeneous infinite medium described by $\epsilon_2(\omega)$, requires the resolution of the Poisson's equation for the electrostatic potential[17]

$$\nabla\left[\epsilon(\boldsymbol{r},\omega)\nabla\phi(\boldsymbol{r},\omega)\right] = -4\pi\rho^{\text{ext}}(\boldsymbol{r},\omega), \tag{1}$$

where

$$\epsilon(\boldsymbol{r},\omega) = \begin{cases} \epsilon_1(\omega) & \text{for } \boldsymbol{r} \text{ inside the particle } (\Omega_1), \\ \epsilon_2(\omega) & \text{for } \boldsymbol{r} \text{ outside the particle } (\Omega_2), \end{cases}$$

and $\rho^{\text{ext}}(\boldsymbol{r},\omega)$ is the external charge density for the test charge. The electrostatic potential in the presence of the particle is

given by[17]

$$\phi(\boldsymbol{r},\omega) = \phi^{\infty}(\boldsymbol{r},\omega) + \phi^{\text{bound}}(\boldsymbol{r},\omega), \tag{2}$$

with

$$\phi^{\infty}(\boldsymbol{r},\omega) = \int d\boldsymbol{r}' \frac{\rho^{\text{ext}}(\boldsymbol{r}',\omega)}{\epsilon(\boldsymbol{r}',\omega)|\boldsymbol{r}-\boldsymbol{r}'|} \tag{3}$$

and

$$\phi^{\text{bound}}(\boldsymbol{r},\omega) = \oint d\boldsymbol{s} \frac{\sigma(\boldsymbol{s},\omega)}{|\boldsymbol{r}-\boldsymbol{s}|}, \tag{4}$$

where $\sigma(\boldsymbol{s},\omega)$ is the single layer of electric charges distributed over the boundary of the particle and verifies[17]

$$2\pi\lambda(\omega)\sigma(\boldsymbol{s},\omega) = \boldsymbol{n}\cdot\nabla\phi^{\infty}(\boldsymbol{s},\omega) + \mathcal{P}\oint d\boldsymbol{s}' F(\boldsymbol{s},\boldsymbol{s}')\sigma(\boldsymbol{s}',\omega), \tag{5}$$

where $\mathcal{P}$ gives the Cauchy principal value (from now, we shall forget to mention the symbol $\mathcal{P}$ to simplify the expressions obtained) and

$$\lambda(\omega) = \frac{\epsilon_2(\omega)+\epsilon_1(\omega)}{\epsilon_2(\omega)-\epsilon_1(\omega)} \tag{6}$$

is a complex function for realistic materials and

$$F(\boldsymbol{s},\boldsymbol{s}') = -\frac{\boldsymbol{n}\cdot(\boldsymbol{s}-\boldsymbol{s}')}{|\boldsymbol{s}-\boldsymbol{s}'|^3} \tag{7}$$

is the normal derivative of the free-space Green's function at the boundary of the particle for $\boldsymbol{s} \neq \boldsymbol{s}'$ and $\boldsymbol{n}$ is the normal vector at the boundary at $\boldsymbol{s}$.

The eigenmodes of the system are obtained when the source-term of Eq. (5) is zero[17]

$$2\pi\lambda_i\sigma^i(\boldsymbol{s}) = \oint d\boldsymbol{s}' F(\boldsymbol{s},\boldsymbol{s}')\sigma^i(\boldsymbol{s}'), \tag{8}$$

where the right eigenmodes $\sigma^i(\boldsymbol{s})$ form a complete basis set that satisfies the unusual orthogonality property[25]

$$\oint d\boldsymbol{s}\oint d\boldsymbol{s}' \frac{\sigma^i(\boldsymbol{s})\sigma^j(\boldsymbol{s}')^*}{|\boldsymbol{s}-\boldsymbol{s}'|} = \delta_{ij}. \tag{9}$$

As reported in Ref. 18, if the boundary of the particle is not smooth, it is preferable to introduce the potential for the electric displacement (such as $\boldsymbol{D} = -\nabla\tilde{\phi}$, where $\boldsymbol{D}$ and $\tilde{\phi}$ are respectively the electric displacement and related potential) instead of the well-known potential for the electric field. This potential can be represented by a dipolar distribution of density $\tau(\boldsymbol{s},\omega)$ distributed over the boundary of the particle and verifying[18]

$$2\pi\lambda_i\tau^i(\boldsymbol{s}) = \oint d\boldsymbol{s}' F(\boldsymbol{s}',\boldsymbol{s})\tau^i(\boldsymbol{s}'). \tag{10}$$

Together with $\sigma^i(\boldsymbol{s})$, they form a complete biorthogonal basis set[24]

$$\oint d\boldsymbol{s}\sigma^i(\boldsymbol{s})\tau^j(\boldsymbol{s}) = \delta_{ij}. \tag{11}$$

Notice that Eq. (8) [or Eq. (10)] depends only on the geometry of the system and not on its composition and thus is valid in particular for realistic lossy materials (for which $\Im[\epsilon_{1,2}(\omega)] \neq 0$). Further, as already noted in Ref. 24, this equation is invariant with respect to the scaling of the dimensions of the material. For the reasons mentioned above, we shall call *geometric eigenmodes* the solutions of Eq. (8) [or Eq. (10)] that are well defined even in lossy materials. More details about Eqs. (8) and (10) can be found in Ref. 25.

III. MODAL DECOMPOSITIONS OF THE SCALAR GREEN'S FUNCTION

A. Modal decomposition in terms of $\phi\tilde{\phi}$

By using Eq. (4) and the orthogonality property (11) between $\sigma^i(\boldsymbol{s})$ and $\tau^i(\boldsymbol{s})$ and the expansion of $\sigma(\boldsymbol{s},\omega)$ in terms of $\sigma^i(\boldsymbol{s})$,[17] one can show that the boundary Green's function for the potential is written as

$$G^{\text{bound}}(\boldsymbol{r},\boldsymbol{r}',\omega) = \frac{1}{2\pi}\frac{1}{\epsilon(\boldsymbol{r}',\omega)}\sum_i \frac{\phi^{\text{bound},i}(\boldsymbol{r})\tilde{\phi}^{\text{bound},i}(\boldsymbol{r}')}{\lambda(\omega)-\lambda_i}, \tag{12}$$

with

$$\tilde{\phi}^{\text{bound},i}(\boldsymbol{r}) = \oint d\boldsymbol{s}\boldsymbol{n}\cdot\nabla\left(\frac{1}{|\boldsymbol{r}-\boldsymbol{s}|}\right)\tau^i(\boldsymbol{s}) \tag{13}$$

is the double layer potential due to the eigendipole density $\tau^i(\boldsymbol{s})$ and

$$\phi^{\text{bound},i}(\boldsymbol{r}) = \oint d\boldsymbol{s}\frac{\sigma^i(\boldsymbol{s})}{|\boldsymbol{r}-\boldsymbol{s}|} \tag{14}$$

is the single layer potential due to the eigencharge density $\sigma^i(\boldsymbol{s})$.

B. Modal decomposition in terms of $\phi\phi^*$

In a similar way, by using the orthogonality property (9) between the $\sigma^i(\boldsymbol{s})$, we get a new modal decomposition of the boundary Green's function:

$$G^{\text{bound}}(\boldsymbol{r},\boldsymbol{r}',\omega) = \frac{1}{\epsilon(\boldsymbol{r}',\omega)}\sum_i\left[\frac{p(1+p\lambda_i)}{\lambda(\omega)-\lambda_i}\right]\phi^{\text{bound},i}(\boldsymbol{r})\phi^{\text{bound},i}(\boldsymbol{r}')^*, \tag{15}$$

where

$$p = \begin{cases} -1 & \text{if } \boldsymbol{r}' \in \Omega_1, \\ 1 & \text{if } \boldsymbol{r}' \in \Omega_2. \end{cases} \tag{16}$$

It is useful to remember here that the above expressions (potential, Green's function, etc.) have been derived in the nonretarded approximation without imposing boundary conditions on the potential. Therefore it is remarkable that the electrostatic potential calculated from the total charge density is identical to that obtained by Stockman *et al.* in Ref. 27 (see also Ref. 28) from the Poisson's equation but imposing homogeneous Dirichlet-Neumann's boundary conditions and where the spectral parameter $s = (1+\lambda)/2$ is used instead of λ. Finally, note also that the expression of the Green's function (15) is compatible to that introduced by Stockman *et al.* in Ref. 28 through a rescaling of the eigenpotentials.

IV. MODAL DECOMPOSITIONS OF THE DYADIC GREEN'S TENSOR

A. Modal decomposition in terms of $E \otimes D$

In the nonretarded approximation ($c \to \infty$), the dyadic Green's tensor for the electric field can be obtained from the scalar Green's function by using the relation

$$\overleftrightarrow{W}^{\text{bound}}(\boldsymbol{r},\boldsymbol{r}',\omega) = \frac{1}{4\pi\omega^2}\nabla\nabla' G^{\text{bound}}(\boldsymbol{r},\boldsymbol{r}',\omega). \quad (17)$$

By substituting Eq. (12) in Eq. (17), we get a modal decomposition of the dyadic Green's tensor for $\boldsymbol{r}'$ inside or outside the particle:

$$\overleftrightarrow{W}^{\text{bound}}(\boldsymbol{r},\boldsymbol{r}',\omega) = \frac{1}{8\pi^2\omega^2}\frac{1}{\epsilon(\boldsymbol{r}',\omega)}\sum_i \frac{\boldsymbol{E}^{\text{bound},i}(\boldsymbol{r})\otimes\boldsymbol{D}^{\text{bound},i}(\boldsymbol{r}')}{\lambda(\omega)-\lambda_i}, \quad (18)$$

where $\otimes$ gives the tensorial product and

$$\boldsymbol{D}^{\text{bound},i}(\boldsymbol{r}) = -\nabla\tilde{\phi}^{\text{bound},i}(\boldsymbol{r}) \quad (19)$$

is the electric displacement due to the dipole density $\tau^i(\boldsymbol{s})$ and $\boldsymbol{E}^{\text{bound},i}(\boldsymbol{r})$ is the electric field due to the charge density $\sigma^i(\boldsymbol{s})$.

B. Modal decomposition in terms of $E \otimes E^*$

An equivalent expansion can be found by using rather the expansion (15), we get

$$\overleftrightarrow{W}^{\text{bound}}(\boldsymbol{r},\boldsymbol{r}',\omega) = \frac{1}{4\pi\omega^2}\frac{1}{\epsilon(\boldsymbol{r}',\omega)}\sum_i\left[\frac{p(1+p\lambda_i)}{\lambda(\omega)-\lambda_i}\right] \times \boldsymbol{E}^{\text{bound},i}(\boldsymbol{r})\otimes\boldsymbol{E}^{\text{bound},i}(\boldsymbol{r}')^*. \quad (20)$$

The modal decomposition (20) is similar to the modal decomposition that appears usually in photonics where the dyadic Green's tensor is expressed in terms of the normalized electric fields associated with the electromagnetic eigenmodes of the structure and derived from the Helmholtz's equation for nondissipative structures:[29]

$$\overleftrightarrow{W}(\boldsymbol{r},\boldsymbol{r}',\omega) = \sum_i \frac{\boldsymbol{E}^i(\boldsymbol{r},\omega_i)\otimes\boldsymbol{E}^i(\boldsymbol{r}',\omega_i)^*}{\omega^2-\omega_i^2}, \quad (21)$$

where ω_i is the eigenfrequency of the mode i. Note, however, that our expression has been established in the nonretarded approximation and in the presence of dissipation while usually such a decomposition is performed in the retarded case without dissipation [see Eq. (21)]. More, the energy squared and eigenenergies are replaced by the dimensionless quantities $2\pi\lambda \in \mathbb{C}$ and $2\pi\lambda_i \in \mathbb{R}$, respectively. The correspondence with the standard modal decomposition of the dyadic Green's tensor well-known in photonics is synthetically summarized by

$$\begin{cases} \omega^2 \in \mathbb{R} \leftrightarrow 2\pi\lambda \in \mathbb{C}, \\ \omega_i^2 \in \mathbb{R} \leftrightarrow 2\pi\lambda_i \in \mathbb{R}, \\ 1 \leftrightarrow \dfrac{2\pi p(1+p\lambda_i)}{4\pi\epsilon(\boldsymbol{r}',\omega)\omega^2}. \end{cases} \quad (22)$$

By using the divergence theorem[30] and the orthogonality property between the $\sigma^i(\boldsymbol{s})$, one can show that the electric eigenfields verify the normalization property (see Appendix A)

$$\int_{\Omega_1} d\boldsymbol{r}|\boldsymbol{E}^{\text{bound},i}(\boldsymbol{r})|^2 + \int_{\Omega_2} d\boldsymbol{r}|\boldsymbol{E}^{\text{bound},i}(\boldsymbol{r})|^2 = 4\pi. \quad (23)$$

A direct comparison between purely photonic and quasistatic expression will be done later on when discussing the compared EMLDOS. Notice that all the previous quantities are well-known in the literature but their expressions in terms of $\sigma^i(\boldsymbol{s})$ and $\tau^i(\boldsymbol{s})$ have never been derived before to the best of our knowledge.

V. GEOMETRIC GREEN'S FUNCTION

Here, we define a quantity that was not reported in the literature to the best of our knowledge. Its interest will be made obvious later (see Sec. VIII). This is the Green's function defined from Eq. (5) by

$$2\pi\lambda g(\boldsymbol{s},\boldsymbol{s}'',\lambda) - \oint d\boldsymbol{s}' F(\boldsymbol{s},\boldsymbol{s}')g(\boldsymbol{s}',\boldsymbol{s}'',\lambda) = \delta(\boldsymbol{s}-\boldsymbol{s}''), \quad (24)$$

where the source-term has been replaced by the boundary delta function $\delta(\boldsymbol{s}-\boldsymbol{s}'')$. The formal expression of $g(\boldsymbol{s},\boldsymbol{s}',\lambda)$ can be found through the right eigenmodes $\sigma^i(\boldsymbol{s})$ by using the expansion

$$g(\boldsymbol{s},\boldsymbol{s}',\lambda) = \sum_i a_i(\boldsymbol{s}',\lambda)\sigma^i(\boldsymbol{s}). \quad (25)$$

Substituting Eq. (25) in Eq. (24), then multiplying by the left eigenmodes $\tau^j(\boldsymbol{s})$ and integrating with respect to $\boldsymbol{s}$, we get

$$g(\boldsymbol{s},\boldsymbol{s}',\lambda) = \frac{1}{2\pi}\sum_i \frac{\sigma^i(\boldsymbol{s})\tau^i(\boldsymbol{s}')}{\lambda-\lambda_i}, \quad (26)$$

where from Eq. (11),

$$\oint d\boldsymbol{s}\sigma^i(\boldsymbol{s})\tau^i(\boldsymbol{s}) = 1. \quad (27)$$

As the geometric eigenmodes are independent of the energy and dielectric function of the underlying media but just depend on the shape of the particle, the previous Green's function only depends on the shape of the particle. Therefore this Green's function is called *geometric Green's function*. Furthermore, the expansion (26) is very similar to a standard modal decomposition but some differences have to be noted: the geometric Green's function is written in terms of the eigenmodes (charges and dipoles) and it is defined only at the surface of the particle and is therefore intrinsically linked to the physics of the surface excitations of the particle, while the standard Green's functions are defined in full space. Again, the energy and the eigenenergies are replaced by the dimensionless quantities $2\pi\lambda \in \mathbb{C}$ and $2\pi\lambda_i \in \mathbb{R}$, respectively. The energy eigenmodes that typically appear [e.g., see numerator of Eq. (21)], which are conjugated to each other, are replaced here by charges and dipoles distributed at the surface of the particle and which are defined by two equations dual to each other [see Eqs. (8) and (10)]. Finally, note that Eq. (26) has been derived by using an usual method[30] from an unique eigenvalues equation for which the charges and dipoles are the eigenmodes, whereas to derive the expressions (12), (15), (18), and (20), we have not explicitly used any eigenvalues

equations for which the potential or the electric field would be the eigenmodes with $2\pi\lambda_i$ as eigenvalue. Note that despite the differences in the modal decompositions derived above (for the scalar Green's function, the dyadic Green's tensor and the geometric Green's function), they have all the same simple poles that are the real eigenvalues $2\pi\lambda_i$.

VI. ELECTROMAGNETIC LOCAL DENSITY OF STATES

A. EMLDOS: a modal decomposition

Joulain *et al*. have shown in Ref. 13, using the fluctuation-dissipation theorem, that the electromagnetic local density of states (EMLDOS) of a particle is formally obtained by taking the imaginary part of the dyadic Green's tensor for the electric field (its magnetic part is irrelevant above the Infra-Red (IR) region):

$$\overleftrightarrow{\rho}^{\mathrm{EM}}(\boldsymbol{r},\omega) = -\frac{2\omega}{\pi}\Im\{[\overleftrightarrow{\boldsymbol{W}}^{\mathrm{bound}}(\boldsymbol{r},\boldsymbol{r},\omega)]\}. \tag{28}$$

As we will see later, the three diagonal components of $\overleftrightarrow{\rho}^{\mathrm{EM}}(\boldsymbol{r},\omega)$ are directly related to the quantity measured in EELS or SNOM experiments. By substituting Eq. (20) in Eq. (28), we obtain

$$\overleftrightarrow{\rho}^{\mathrm{EM}}_{\alpha\alpha}(\boldsymbol{r},\omega) = \overleftrightarrow{\rho}^{\mathrm{SP}}_{\alpha\alpha}(\boldsymbol{r},\omega) + \overleftrightarrow{\rho}^{\mathrm{beg}}_{\alpha\alpha}(\boldsymbol{r},\omega) \tag{29}$$

with

$$\overleftrightarrow{\rho}^{\mathrm{SP}}_{\alpha\alpha}(\boldsymbol{r},\omega) = \frac{1}{2\pi^2\omega}\sum_i \Im\left[-g_i(\omega)\right]\left|\boldsymbol{E}^{\mathrm{bound},i}_{\alpha}(\boldsymbol{r})\right|^2 \tag{30}$$

and

$$\overleftrightarrow{\rho}^{\mathrm{beg}}_{\alpha\alpha}(\boldsymbol{r},\omega) = -\frac{1}{2\pi^2\omega}\sum_i \Im\left[-\frac{1}{\epsilon_\mu(\omega)}\right]\left|\boldsymbol{E}^{\mathrm{bound},i}_{\alpha}(\boldsymbol{r})\right|^2, \tag{31}$$

where $\mu = 1$ if $\boldsymbol{r} \in \Omega_1$ and $\mu = 2$ if $\boldsymbol{r} \in \Omega_2$ and where the relation

$$\frac{1}{\epsilon(\boldsymbol{r}',\omega)}\frac{p(1+p\lambda_i)}{\lambda(\omega)-\lambda_i} = g_i(\omega) - \frac{1}{\epsilon_\mu(\omega)} \tag{32}$$

with

$$g_i(\omega) = \frac{2}{\epsilon_1(\omega)(1+\lambda_i)+\epsilon_2(\omega)(1-\lambda_i)} \tag{33}$$

has been used. $\overleftrightarrow{\rho}^{\mathrm{SP}}_{\alpha\alpha}(\boldsymbol{r},\omega)$ is related to the surface excitations (surface plasmons) of the particle and $\overleftrightarrow{\rho}^{\mathrm{beg}}_{\alpha\alpha}(\boldsymbol{r},\omega)$ is called *begrenzung term*. This term corresponds to the modification of the bulk contribution (corresponding to the EMLDOS in an infinitely extended volume of local dielectric function ϵ_1 or ϵ_2) due to the presence of the boundaries. Experimentally, it manifests itself by a decrease of the EELS signal when one approach the boundary of the particle at the volume plasmon resonance (see Sec. IX).

While the expression of the EMLDOS for photonic structures is well-known, our formalism has allowed us to derive, for the first time, an universal expression of the EMLDOS for any plasmonic structure in terms of the geometric eigenmodes of the particle well defined in dissipative structures. As reported in Ref. 31 in the relativistic case, the LDOS inside the particle infinitely close to the boundary is singular in the presence of dissipative materials. In the quasistatic limit, the expression (17) exhibits such singularities. Indeed, in the case where $\boldsymbol{r}'$ is defined in full space including the boundary of the particle, an additional contribution proportionnal to $\nabla'[1/\epsilon(\boldsymbol{r}',\omega)]$ appears in the dyadic Green's tensor. This contribution gives zero inside or outside the particle for homogeneous media but it gives a singular value at the boundary due to the discontinuity of $\epsilon(\boldsymbol{r}',\omega)$. Concerning the EMLDOS, this contribution disappears everywhere in nonlossy materials but it gives a singular value at the boundary of the particle in lossy materials. More generally, such kind of divergences are unphysical and related to the fact that all calculations have been performed in the local approximation. It is known that taking into account the spatial dispersion of the dielectric constant usually removes the divergence, and that the error in considering the local response is usually not relevant but for a few tenth of nanometer close to the surface. A similar discussion follows later in the case of EELS and SNOM.

B. EMLDOS in the Drude's model

To make more intuitive the expression of the EMLDOS and to compare the expression obtained with the one well-known in photonics, we suppose that the particle is composed of a medium described by a dissipative Drude's model: $\epsilon_1(\omega) = 1 - \omega_p^2/\omega(\omega + i\Gamma)$ (ω_p is the plasma pulsation of the medium and Γ plays for the damping) and embedded in vacuum: $\epsilon_2(\omega) = 1$. From now, we will consider for simplicity rather the trace of the EMLDOS as it appears frequently in literature. After some calculations, we get

$$\rho^{\mathrm{SP}}(\boldsymbol{r},\omega) \equiv \mathrm{Tr}[\overleftrightarrow{\rho}^{\mathrm{SP}}(\boldsymbol{r},\omega)] \equiv \sum_{\alpha=x,y,z}\overleftrightarrow{\rho}^{\mathrm{SP}}_{\alpha\alpha}(\boldsymbol{r},\omega)$$
$$= \frac{1}{2\pi^2}\sum_i \frac{\Gamma\tilde{\omega}_i^2}{\Gamma^2\omega^2 + \left(\omega^2 - \tilde{\omega}_i^2\right)^2}|\boldsymbol{E}^{\mathrm{bound},i}(\boldsymbol{r})|^2, \tag{34}$$

where $\omega_i = \frac{\omega_p}{\sqrt{2}}\sqrt{1+\lambda_i}$.

In the nondissipative limit, by using the identity $\lim_{a\to 0}\frac{a}{a^2+x^2} = \pi\delta(x)$, Eq. (34) becomes

$$\rho^{\mathrm{SP}}(\boldsymbol{r},\omega) = \frac{1}{4\pi}\sum_i \delta(\omega-\omega_i)|\boldsymbol{E}^{\mathrm{bound},i}(\boldsymbol{r})|^2, \tag{35}$$

where the normalization of the electric field in full space is 4π (see Appendix A). Although derived from different equations and different approximations, the expression (35) for the nondissipative EMLDOS is similar to the well-known EMLDOS in photonics,[29] i.e., $\rho(\boldsymbol{r},\omega) = \sum_i \delta(\omega - \omega_i)|\boldsymbol{E}^i(\boldsymbol{r},\omega_i)|^2$. Nevertheless, some differences have to be noted: in the photonic case, the EMLDOS is written in terms of the normalized electric fields associated with the energy modes of the structure derived from the retarded Helmholtz's equation and based on strict boundary conditions (infinitely reflective surfaces). Note also that in the nondissipative limit, an energy excitation ω_i can be associated to the geometric eigenmode i as if it were an eigenenergy for this mode while the true eigenvalue is λ_i. In this limit, a geometric eigenmode can be considered as a mode defined by a single energy. It is not surprising to note that this correspondence becomes

ambiguous for dissipative systems since, in this case, the delta function peaked at ω_i is replaced by a Lorentzian function [see Eq. (34)] and thus that an infinity of energy excitations can be associated to a single geometric eigenmode. Experimentally, this will involve an exponential decay in time (and thus a finite lifetime) of the geometric eigenmodes excited selectively by injecting energy (e.g., in EELS experiments) into the system. Although the eigenmodes can be clearly defined, using the regular (energy dependent) EMLDOS to characterize them seems thus slightly inappropriate when dissipation comes into play. In Sec. VII, we will define a LDOS for the geometric eigenmodes and the eigenvalues λ_i forgetting the "standard" variable energy, which will allow to solve this problem for dissipative systems.

C. Number of accessible geometric eigenmodes

To check the validity of the modal decompositions (30) and (31), we can consider again the trace of $\overleftrightarrow{\rho}^{\mathrm{EM}}(\boldsymbol{r},\omega)$ and calculate its integral over ω and $\boldsymbol{r}$: $\rho^{\mathrm{EM}} \equiv \int d\boldsymbol{r} \int_0^{+\infty} d\omega \rho^{\mathrm{EM}}(\boldsymbol{r},\omega)$. For the contribution related to the surface excitations, it is expected that the resulting quantity is the total number of accessible surface excitations of the particle. Here, we will check this statement without introducing explicit energy dependence in the dielectric functions of the underlying media.

From Eq. (29), we have

$$\rho^{\mathrm{EM}} = \rho^{\mathrm{SP}} + \rho^{\mathrm{beg},1} + \rho^{\mathrm{beg},2}, \tag{36}$$

where

$$\rho^{\mathrm{SP}} = \frac{1}{2\pi^2} \sum_{i=1}^{N} \int_0^{+\infty} \frac{d\omega}{\omega} \Im\left[-g_i(\omega)\right] \left\{ \int_{\Omega_1} d\boldsymbol{r} |\boldsymbol{E}^{\mathrm{bound},i}(\boldsymbol{r})|^2 + \int_{\Omega_2} d\boldsymbol{r} |\boldsymbol{E}^{\mathrm{bound},i}(\boldsymbol{r})|^2 \right\}; \tag{37}$$

$$\rho^{\mathrm{beg},1} = -\frac{1}{2\pi^2} \sum_{i=1}^{N} \int_0^{+\infty} \frac{d\omega}{\omega} \Im\left[-\frac{1}{\epsilon_1(\omega)}\right] \times \int_{\Omega_1} d\boldsymbol{r} |\boldsymbol{E}^{\mathrm{bound},i}(\boldsymbol{r})|^2 \tag{38}$$

and

$$\rho^{\mathrm{beg},2} = -\frac{1}{2\pi^2} \sum_{i=1}^{N} \int_0^{+\infty} \frac{d\omega}{\omega} \Im\left[-\frac{1}{\epsilon_2(\omega)}\right] \times \int_{\Omega_2} d\boldsymbol{r} |\boldsymbol{E}^{\mathrm{bound},i}(\boldsymbol{r})|^2. \tag{39}$$

The integrals over ω are performed by using the first Kramers-Kronig's relation.[32] After some calculations (see Appendix B), we find

$$\int_0^{+\infty} \frac{d\omega}{\omega} \Im\left[-g_i(\omega)\right] = \frac{\pi}{2} \tag{40}$$

and the well-known identities[32]

$$\int_0^{+\infty} \frac{d\omega}{\omega} \Im\left[-\frac{1}{\epsilon_1(\omega)}\right] = \int_0^{+\infty} \frac{d\omega}{\omega} \Im\left[-\frac{1}{\epsilon_2(\omega)}\right] = \frac{\pi}{2}. \tag{41}$$

By collecting these results, we obtain

$$\rho^{\mathrm{SP}} = \frac{1}{4\pi} \sum_{i=1}^{N} \left\{ \int_{\Omega_1} d\boldsymbol{r} |\boldsymbol{E}^{\mathrm{bound},i}(\boldsymbol{r})|^2 + \int_{\Omega_2} d\boldsymbol{r} |\boldsymbol{E}^{\mathrm{bound},i}(\boldsymbol{r})|^2 \right\}, \tag{42}$$

$$\rho^{\mathrm{beg},1} = -\frac{1}{4\pi} \sum_{i=1}^{N} \int_{\Omega_1} d\boldsymbol{r} |\boldsymbol{E}^{\mathrm{bound},i}(\boldsymbol{r})|^2, \tag{43}$$

$$\rho^{\mathrm{beg},2} = -\frac{1}{4\pi} \sum_{i=1}^{N} \int_{\Omega_2} d\boldsymbol{r} |\boldsymbol{E}^{\mathrm{bound},i}(\boldsymbol{r})|^2. \tag{44}$$

The integrals over $\boldsymbol{r}$ are obtained by using the normalization relations (A5) and (A6) derived in Appendix A. We get

$$\rho^{\mathrm{SP}} = N(\text{total number of modes}); \tag{45}$$

$$\rho^{\mathrm{beg},1} = -\frac{1}{2} \sum_{i=1}^{N} (1 - \lambda_i); \tag{46}$$

$$\rho^{\mathrm{beg},2} = -\frac{1}{2} \sum_{i=1}^{N} (1 + \lambda_i). \tag{47}$$

As expected, we get the total number of states (geometric eigenmodes) after integration of $\rho^{\mathrm{SP}}(\boldsymbol{r},\omega)$. Otherwise, the total contribution associated to the begrenzung effect gives

$$\rho^{\mathrm{beg}} \equiv \rho^{\mathrm{beg},1} + \rho^{\mathrm{beg},2} = -N. \tag{48}$$

The negative sign that appears in the right-hand side is not an artifact of the calculation but reflects the fact that the "begrenzung states" have been "drawn" in a reservoir of available states and that there are as many begrenzung states as geometric eigenmodes (N). More, unlike ρ^{SP} (or ρ^{beg}), the expressions (46) and (47) show that $\rho^{\mathrm{beg},1} \neq \rho^{\mathrm{beg},2}$ and that these quantities depend on the eigenvalues except when $\lambda_i = 0$ (case of an infinite planar interface between the two media). Again, our formalism allowed us to derive this result, not reported before to the best of our knowledge. Obviously these results are unchanged if the particle is described, as before, by a Drude's model or even another more complex model.

VII. GEOMETRIC LOCAL DENSITY OF STATES (GLDOS)

The EMLDOS derived in Sec. VI is expressed in terms of the geometric eigenmodes independent of the energy and the nature of the underlying media. However, the EMLDOS is naturally defined in terms of energy and depends on the nature of the media through the dielectric functions. Here, we define a LDOS for the geometric eigenmodes (GLDOS) in terms of the natural variable of the problem which is not the energy but λ [see Eq. (5)]. As we will see later, the result obtained will remain valid whatever the nature of the media and the underlying excitations (plasmons, interband transitions, etc.) Therefore, each geometric eigenmode associated to the eigenvalue λ_i and appearing in this LDOS will be defined unambiguously whatever the media. This is also true in the particular case of plasmonic dissipative structures.

As we said above, the expression (26) of the geometric Green's function is very similar to a standard modal decomposition but nevertheless some differences were noted: the energy (real) that appears in the standard modal decomposition and which is the variable of interest is replaced here by

the dimensionless quantity λ, which is complex for realistic physical systems (with dissipation). This makes *a priori* difficult the use of the geometric Green's function to define the GLDOS. However, to achieve this, we can reason by analogy with the photonic case, where the EMLDOS for the photonic eigenmodes is formally expressed in terms of the dyadic Green's tensor. This will allow us to define a LDOS for the geometric eigenmodes, in the complex plane subtended by λ rather than by a plane subtended by an energy. For a nondissipative photonic structure described by the electromagnetic eigenmodes $\boldsymbol{E}^i(\boldsymbol{r},\omega_i)$ and the eigenenergies ω_i, the EMLDOS is written as[29]

$$\rho(\boldsymbol{r},\omega) = \sum_i |\boldsymbol{E}^i(\boldsymbol{r},\omega_i)|^2 \delta(\omega-\omega_i) \tag{49}$$

and it can be formally obtained from the dyadic Green's tensor derived from the retarded Helmholtz's equation. The δ-function $\delta(\omega-\omega_i)$, where $\omega,\omega_i \in \mathcal{R}$, which allows to count all the modes one by one, has to be replaced, here, by its analog in the "complex world", i.e.,

$$\delta(\omega-\omega_i) \leftrightarrow \frac{1}{\lambda-\lambda_i}. \tag{50}$$

This analogy is apparent when we notice that $\delta(\omega-\omega_i)$ and $1/(\lambda-\lambda_i)$ act almost similarly on a test function f,

$$\int_0^{+\infty} d\omega \delta(\omega-\omega_i) f(\omega) = f(\omega_i)$$

and

$$\oint_{\gamma_i} d\lambda \frac{f(\lambda)}{\lambda-\lambda_i} = 2\pi i f(\lambda_i),$$

where the last integral is defined in the complex plane and γ_i is a contour of integration that embraces the simple pole λ_i. It is now clear that the Green's function given by the expansion (26) can be used to define formally the geometric local density of states of the particle. The integration over the energy ω, typically done on the standard EMLDOS, giving the total number of modes per unit volume has to be replaced by an integration, in the complex plane, with respect to the complex variable λ and the contour of integration γ should embrace the segment $[-1,1]$ in which the poles of $g(\boldsymbol{s},\boldsymbol{s},\lambda)$ take their values. The result will be a number of geometric modes per unit surface. Thanks to the analyticity of the geometric Green's function and by the Cauchy's theorem, if we deform the contour of integration in the union of small contours γ_i around the poles (see Fig. 1), then the value of the integral will

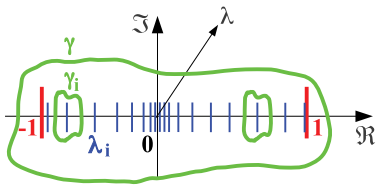

FIG. 1. (Color online) Distribution of the eigenvalues λ_i between -1 and 1. γ_i is a contour of integration that embraces the eigenvalue λ_i and γ embraces all of them.

not change. We get successively

$$\begin{aligned}\Im\left[\oint_\gamma d\lambda g(\boldsymbol{s},\boldsymbol{s}',\lambda)\right] &= \Im\left[\oint_{\cup_i\gamma_i} d\lambda g(\boldsymbol{s},\boldsymbol{s}',\lambda)\right] \\ &= \sum_{i=1}^N \Im\left[\oint_{\gamma_i} d\lambda g(\boldsymbol{s},\boldsymbol{s}',\lambda)\right] \\ &= \sum_{i=1}^N \Im\{2\pi i \mathrm{Res}[g(\boldsymbol{s},\boldsymbol{s}',\lambda),\lambda_i]\} \\ &= \sum_{i=1}^N \sigma^i(\boldsymbol{s})\tau^i(\boldsymbol{s}'),\end{aligned} \tag{51}$$

where Res gives the residue of $g(\boldsymbol{s},\boldsymbol{s}',\lambda)$ at λ_i. The previous calculation shows that we can formally identify the total number of geometric modes per unit surface of the particle $\rho^{\mathrm{GEO}}(\boldsymbol{s})$ by using the relation

$$\rho^{\mathrm{GEO}}(\boldsymbol{s}) = \Im\left[\oint_\gamma d\lambda g(\boldsymbol{s},\boldsymbol{s},\lambda)\right]. \tag{52}$$

Also, the integration over the boundary of the particle gives the total number of accessible states

$$\begin{aligned}\oint d\boldsymbol{s}\rho^{\mathrm{GEO}}(\boldsymbol{s}) &= \sum_{i=1}^N \overbrace{\oint d\boldsymbol{s}\sigma^i(\boldsymbol{s})\tau^i(\boldsymbol{s})}^{\delta_{ii}=1} \\ &= N(\text{total number of states}),\end{aligned} \tag{53}$$

where the biorthogonality property (11) between the eigencharges and dipoles has been used.

The calculation that we just performed shows that the geometric Green's function is quite suitable to define a new type of local density of states that depends only on the shape of the particle (GLDOS) and that is independent of the nature of the media. Unlike the EMLDOS defined in terms of energy and whose the physical interpretation in terms of number of accessible "energy" modes is ambiguous for dissipative systems since then an infinity of energy can be associated to a single geometric eigenmode (see Sec. VI B), the interpretation of the GLDOS in terms of accessible number of geometric modes (defined by the eigenvalue λ_i instead of the energy) may still be maintained, without any ambiguity for any structures, like dissipative metals underlying plasmonic waves, or insulators. Here, we used the natural variable of the problem λ but the price to pay to use it, by analogy with the energy that appears in the standard case, was to define the GLDOS in the complex plane subtended by λ.

VIII. LINK BETWEEN THE STANDARD GREEN'S FUNCTIONS AND THE GEOMETRIC GREEN'S FUNCTION

All the standard Green's functions we have introduced above (scalar Green's function and dyadic Green's tensor) can be obtained through integrations and/or derivations operations of the geometric Green's function, placing it to the rank of "generator" function and therefore making it more fundamental than the other. The diagram below summarizes how the various process allow to move from one to another of these

Green's functions:

$$\boxed{g(\boldsymbol{s},\boldsymbol{s}',\lambda)} \qquad \text{(GLDOS)}$$
$$\downarrow \frac{1}{\epsilon(\boldsymbol{r}',\omega)} \oint d\boldsymbol{s} \oint d\boldsymbol{s}' \frac{1}{|\boldsymbol{r}-\boldsymbol{s}|}\, \boldsymbol{n}'\cdot\nabla' \frac{1}{|\boldsymbol{r}'-\boldsymbol{s}'|}$$
$$\boxed{G(\boldsymbol{r},\boldsymbol{r}',\omega)} \qquad \text{(EELS)}$$
$$\downarrow \frac{1}{4\pi\omega^2}\nabla\nabla'$$
$$\boxed{\overleftrightarrow{\boldsymbol{W}}(\boldsymbol{r},\boldsymbol{r}',\omega)} \qquad \text{(EELS, SNOM, EMLDOS)}$$

The diagram above implies that all quantities that can be derived from the standard Green's functions (EELS, SNOM, GLDOS, or EMLDOS) can be expressed, in more or less complex ways, depending on the quantity considered, in terms of $g(\boldsymbol{s},\boldsymbol{s}',\lambda)$. The energy dependence arises when we have to specify an energy dispersion for the dielectric functions of the media involved (particle and environment), i.e., when we specify the nature of these media, which is necessary for example for EELS and SNOM since, by nature, these experiments are described in terms of energy. This energy dispersion will cause the loss of the spatial coherence of the geometric eigenmodes and the experimental results for a same geometry may be different depending on the nature of the media (see Sec. XI).

IX. MODAL DECOMPOSITIONS OF EELS

EELS is a technique that has recently shown great success in mapping plasmons in small nanoparticles.[2,3,10,33–38] Determining the EELS as a function of the geometric eigenmodes is therefore of interest in order to clearly understand experiments.

A. EELS in terms of potential

The energy loss probability of a fast electron in the presence of a particle is given, in the nonretarded approximation, by the average value of the imaginary part of the scalar Green's function.[39] For an electron moving along the axis Oz with constant velocity $\boldsymbol{v}$ with impact parameter $\boldsymbol{R}_0=(x_0,y_0)$ and considering only the contributions due to the boundary of the particle, it gives[39]

$$\Gamma^{\text{bound}}(\boldsymbol{R}_0,\omega) = -\frac{1}{\pi}\int_{-\infty}^{\infty} d\boldsymbol{r}\int_{-\infty}^{\infty} d\boldsymbol{r}'\Im[\rho^{\text{ext}}(\boldsymbol{r},\omega)^* \times G^{\text{bound}}(\boldsymbol{r},\boldsymbol{r}',\omega)\rho^{\text{ext}}(\boldsymbol{r}',\omega)], \tag{54}$$

where

$$\rho^{\text{ext}}(\boldsymbol{r},\omega) = -\frac{1}{v}\delta(\boldsymbol{R}-\boldsymbol{R}_0)e^{i\omega/vz} \tag{55}$$

is the charge density associated to the electron in the angular frequencies space and where we noted $\boldsymbol{r}=(\boldsymbol{R},z)$ with $\boldsymbol{R}=(x,y)$. By substituting the modal decomposition (15) in Eq. (54), we obtain

$$\begin{aligned}\Gamma^{\text{bound}}(\boldsymbol{R}_0,\omega) &= -\frac{1}{\pi v^2}\sum_i \Im\Bigg[g_i(\omega)\int_{-\infty}^{+\infty} dz\phi^{\text{bound},i}(\boldsymbol{R}_0,z)e^{-i\omega/vz} \times\int_{-\infty}^{+\infty} dz'\phi^{\text{bound},i}(\boldsymbol{R}_0,z')^* e^{i\omega/vz'} \\ &\quad -\int_{-\infty}^{+\infty} dz\phi^{\text{bound},i}(\boldsymbol{R}_0,z)e^{-i\omega/vz} \times\sum_{\mu=1,2}\frac{1}{\epsilon_\mu(\omega)}\int_{L_\mu} dz'\phi^{\text{bound},i}(\boldsymbol{R}_0,z')^* e^{i\omega/vz'}\Bigg],\end{aligned} \tag{56}$$

where L_μ is the length traversed by the electron in the medium μ. By performing the integration over z and z', the previous expression becomes

$$\Gamma^{\text{bound}}(\boldsymbol{R}_0,\omega) = \Gamma^{\text{SP}}(\boldsymbol{R}_0,\omega)+\Gamma^{\text{beg}}(\boldsymbol{R}_0,\omega), \tag{57}$$

where

$$\Gamma^{\text{SP}}(\boldsymbol{R}_0,\omega) = \frac{1}{\pi v^2}\sum_i \Im[-g_i(\omega)]|\phi^{\text{bound},i}(\boldsymbol{R}_0,q)|^2 \tag{58}$$

and

$$\Gamma^{\text{beg}}(\boldsymbol{R}_0,\omega) = \frac{1}{\pi v^2}\sum_i \Im\Bigg[\int_{-\infty}^{+\infty} dz\phi^{\text{bound},i}(\boldsymbol{R}_0,z)e^{-i\omega/vz} \times\sum_{\mu=1,2}\frac{1}{\epsilon_\mu(\omega)}\int_{L_\mu} dz'\phi^{\text{bound},i}(\boldsymbol{R}_0,z')^* e^{i\omega/vz'}\Bigg], \tag{59}$$

with $q=\omega/v$ and where $\phi^{\text{bound},i}(\boldsymbol{R}_0,q)$ is the Fourier transform with respect to z of $\phi^{\text{bound},i}(\boldsymbol{R}_0,z)$.

The first term Γ^{SP} gives the probability that the electron loses the energy ω by exciting the surface modes of the particle and whose the positions of the maxima are given by that of $\Im[-g_i(\omega)]$. The second term Γ^{beg} gives a negative contribution to the probability of loss the energy ω by exciting the volume modes in the different media traversed by the incident electrons (begrenzung effect).

Nonpenetrating trajectory. In the particular case where the trajectory of the electron is not penetrating, that is to say, when the electron moves next the particle, the expression (56) simplifies and becomes

$$\Gamma^{\text{bound}}(\boldsymbol{R}_0,\omega) = -\frac{1}{\pi v^2}\sum_i \Im\left[g_i(\omega)-\frac{1}{\epsilon_2(\omega)}\right]|\phi^{\text{bound},i}(\boldsymbol{R}_0,q)|^2. \tag{60}$$

B. EELS in terms of charge density

In order to obtain expressions easily interpretable and intuitive, we will consider from now only the term associated to the surface excitations of the particle [i.e., $\Gamma^{\text{SP}}(\boldsymbol{R}_0,\omega)$]. By expressing the potential in terms of the eigencharge density, we have successively (with $q=\omega/v$)

$$\begin{aligned}\phi^{\text{bound},i}(\boldsymbol{R}_0,q) &= \int_{-\infty}^{+\infty} dz\phi^{\text{bound},i}(\boldsymbol{R}_0,z)e^{-i\omega/vz} \\ &= \int_{-\infty}^{+\infty} dz e^{-i\omega/vz}\oint d\boldsymbol{s}\frac{\sigma^i(\boldsymbol{s})}{|\boldsymbol{R}_0+z\hat{\boldsymbol{z}}-\boldsymbol{s}|} \\ &= \oint d\boldsymbol{s}\sigma^i(\boldsymbol{s})\int_{-\infty}^{+\infty} dz\frac{e^{-i\omega/vz}}{|\boldsymbol{R}_0+z\hat{\boldsymbol{z}}-\boldsymbol{s}|} \\ &= 2\oint d\boldsymbol{s}\sigma^i(\boldsymbol{s})e^{-i\omega/v\boldsymbol{s}^\parallel}K_0\left(\frac{\omega|\boldsymbol{R}_0-\boldsymbol{s}^\perp|}{v}\right),\end{aligned} \tag{61, 62}$$

where $\boldsymbol{s}^{\perp}$ is the component of $\boldsymbol{s}$ perpendicular to the trajectory of the electron (in the plane xOy) and $s^{\parallel}$ is the component of $\boldsymbol{s}$ along the trajectory of the electron (along Oz): $\boldsymbol{s} = (\boldsymbol{s}^{\perp}, s^{\parallel})$. $\hat{\boldsymbol{z}}$ is an unit vector carried by the axis Oz and K_0 is the Bessel's function of second kind of order 0. Therefore the energy loss probability becomes

$$\Gamma^{\mathrm{SP}}(\boldsymbol{R}_0,\omega) = \frac{4}{\pi v^2}\sum_i \Im\left[-g_i(\omega)\right]\left|\oint d\boldsymbol{s}\sigma^i(\boldsymbol{s})e^{-i\omega/vs^{\parallel}} \times K_0\left(\frac{\omega|\boldsymbol{R}_0-\boldsymbol{s}^{\perp}|}{v}\right)\right|^2. \tag{63}$$

Note that the expression (63) is a reformulation of that obtained by García de Abajo and Aizpurua [see Eq. (18) in Ref. 17], but in this present case highlighting the separate role of $\sigma^i(\boldsymbol{s})$ and the interaction (represented by K_0).

C. EELS in terms of electric field

It is also possible to express the energy loss probability in terms of the electric field along z: $E_z^{\mathrm{bound},i}$. To do it, note that in the real space, the component along z (propagation direction of the electron) of the electric field is written

$$E_z^{\mathrm{bound},i}(\boldsymbol{r}) = -\frac{\partial\phi^{\mathrm{bound},i}(\boldsymbol{r})}{\partial z}, \tag{64}$$

which becomes in the Fourier space along z, with $q = \omega/v$ and noting $\boldsymbol{r} = (\boldsymbol{R},z)$

$$E_z^{\mathrm{bound},i}(\boldsymbol{R},q) = -iq\phi^{\mathrm{bound},i}(\boldsymbol{R},q). \tag{65}$$

Substituting the expression of $\phi^{\mathrm{bound},i}(\boldsymbol{R},q)$ in terms of $E_z^{\mathrm{bound},i}(\boldsymbol{R},q)$ in Eq. (60), we obtain

$$\Gamma^{\mathrm{SP}}(\boldsymbol{R}_0,\omega) = \frac{1}{\pi\omega^2}\sum_i \Im\left[-g_i(\omega)\right]\left|E_z^{\mathrm{bound},i}(\boldsymbol{R}_0,q)\right|^2 \tag{66}$$

or

$$\Gamma^{\mathrm{SP}}(\boldsymbol{R}_0,\omega) = -4\Im[\overleftrightarrow{\boldsymbol{W}}{}^{\mathrm{SP}}_{zz}(\boldsymbol{R}_0,q,\boldsymbol{R}_0,-q)], \quad q=\omega/v, \tag{67}$$

where $\overleftrightarrow{\boldsymbol{W}}{}^{\mathrm{SP}}_{zz}(\boldsymbol{r},\boldsymbol{r}',\omega)$ is obtained from the modal decomposition (20) of the dyadic Green's tensor removing the term corresponding to the begrenzung contribution. We note that expression (67) is compatible with the general relation between the EELS and the EMLDOS already given in Ref. 40.

In this section, EELS has been derived from the scalar Green's function involving only $1/\epsilon(\boldsymbol{r}',\omega)$ which remains finite everywhere. Then, we used the expression obtained in terms of potentials to derive a simplified expression of EELS in terms of electric fields. Therefore the divergence already discussed above (see Sec. VI) has never occurred in our calculation. Moreover, EELS expressed in terms of the dyadic Green's tensor has been derived for a nonpenetrating trajectory and in this case, $\nabla'[1/\epsilon(\boldsymbol{r}',\omega)] = 0$ and there is no divergence to take into account. For a penetrating trajectory, EELS can also be expressed in terms of the dyadic Green's tensor but this requires to consider the singular contribution at the boundary in the dyadic Green's tensor. However, this singularity is integrable since $\nabla'[1/\epsilon(\boldsymbol{r}',\omega)] = 0 + \boldsymbol{n}\,(1/\epsilon_2 - 1/\epsilon_1)\delta_s$, where δ_s is a δ-function, which is zero everywhere except at the boundary of the particle.

The formalism of the modal decomposition that we developed allowed us to derive different expressions of the energy loss probability in the presence of a particle of any shape. Unlike the modal decomposition of the geometric Green's function (26) (or GLDOS), the previous expressions of Γ^{SP} show a clear dependence in energy, especially through the dielectric functions of the media that constitute the particle and its environment and despite the fact that this experimental quantity could be written in terms of the geometric eigenmodes independent of the nature of these media. As we mentioned earlier, this energy dependence will cause the loss of the spatial coherence of the geometric eigenmodes, which will be discussed in Sec. XII.

X. MODAL DECOMPOSITIONS OF SNOM

A. SNOM in terms of electric field

In a simplified way (without taking into account the illumination and detection conditions), it can be shown[12] that the signal detected in scanning near optical microscope experiments (SNOM) is proportional to the temporal average of the energy density emitted in full space by the probed particle. If the probe is modeled by an oscillating dipole at the pulsation ω, that is of the form $\boldsymbol{p}(t) = \boldsymbol{p}_0\cos(\omega t)$, located at the position $\boldsymbol{r} = (\boldsymbol{R}_0,z)$, where $\boldsymbol{R}_0 = (x_0,y_0)$ and oriented in the direction $\alpha = x,y$, or z, then the signal detected due to the presence of the particle is

$$S^{\mathrm{snom}}(\boldsymbol{r},\omega) = -2\pi\omega^3 p_{0\alpha}^2\Im\left[\overleftrightarrow{\boldsymbol{W}}{}^{\mathrm{bound}}_{\alpha\alpha}(\boldsymbol{r},\boldsymbol{r},\omega)\right]. \tag{68}$$

By using the modal decomposition (20) of $\overleftrightarrow{\boldsymbol{W}}{}^{\mathrm{bound}}_{\alpha\alpha}(\boldsymbol{r},\boldsymbol{r},\omega)$ and assuming that the dipole-probe oscillates in the direction z, the expression (68) of the signal measured in SNOM becomes, if we forget the begrenzung term as a simplification,

$$S^{\mathrm{snom}}(\boldsymbol{R}_0,z,\omega) = \frac{\omega}{2}p_{0z}^2\sum_i \Im\left[-g_i(\omega)\right]\left|E_z^{\mathrm{bound},i}(\boldsymbol{R}_0,z)\right|^2. \tag{69}$$

The expression (69) shows that the SNOM signal is a function of the square of the electric field along z measured in the real space, that is to say that SNOM $\propto |E_z^{\mathrm{bound},i}(\boldsymbol{R}_0,z)|^2$. Note that a similar expression, written in terms of the photonic eigenmodes (defined by their eigenenergy), is known in photonics[29] but had never been demonstrated before in plasmonics. In SNOM, for a position fixed $\boldsymbol{R}_0$, the parameter z (distance probe-particle) can be changed by the experimenter. Moreover, the EELS signal is also a function of the square of the electric field along z but it is evaluated in the momentum space (after a Fourier transform along z), that is to say that EELS $\propto |E_z^{\mathrm{bound},i}(\boldsymbol{R}_0,\omega/v)|^2$ [see Eq. (66)] and in this case, the parameter $q = \omega/v$ can be changed by the experimenter by changing the velocity of the incident electrons v. We will discussed again the difference between EELS and SNOM signal later. Notice that general derivations of SNOM signals can be found in Refs. 41 and 42.

B. SNOM in terms of charge density

It is easy to derive an expression of the SNOM signal in terms of the eigencharge densities $\sigma^i(\boldsymbol{s})$ (geometric eigenmodes) from Eq. (69), indeed, we have

$$\begin{aligned} E_z^{\text{bound},i}(\boldsymbol{R}_0,z) &= -\left[\frac{\partial}{\partial z}\oint d\boldsymbol{s}\frac{\sigma^i(\boldsymbol{s})}{|\boldsymbol{r}-\boldsymbol{s}|}\right]_{\boldsymbol{r}=(\boldsymbol{R}_0,z)} \qquad (70)\\ &= \oint d\boldsymbol{s}\frac{\sigma^i(\boldsymbol{s})(z-s_z)}{[(x_0-s_x)^2+(y_0-s_y)^2+(z-s_z)^2]^{3/2}}\\ &= \oint d\boldsymbol{s}\frac{\sigma^i(\boldsymbol{s})(z-s^{\parallel})}{[|\boldsymbol{R}_0-\boldsymbol{s}^{\perp}|^2+(z-s^{\parallel})^2]^{3/2}} \qquad (71)\end{aligned}$$

and thus

$$S^{\text{snom}}(\boldsymbol{R}_0,z,\omega) = \frac{\omega}{2}p_{0z}^2\sum_i \Im[-g_i(\omega)] \times\left|\oint d\boldsymbol{s}\frac{\sigma^i(\boldsymbol{s})(z-s^{\parallel})}{[|\boldsymbol{R}_0-\boldsymbol{s}^{\perp}|^2+(z-s^{\parallel})^2]^{3/2}}\right|^2. \qquad (72)$$

The expression (72) can be compared to that we obtained previously for EELS [see Eq. (63)]. These expressions, written in terms of $\sigma^i(\boldsymbol{s})$, show that in EELS or SNOM experiments, the measured signal is an "image" of the eigencharge density but convolved by a kernel that is different for EELS and SNOM but with the same physical origin (the Coulombian interaction). Note, however, that because of the square which is involved in Eqs. (63) and (72), the EELS and the SNOM do not measure the exact convolved charge density but rather the modulus squared of this charge density convolved. It makes difficult to solve the inverse problem, that is to say the exact determination of the charge densities from EELS or SNOM maps obtained experimentally by deconvolution of the data is difficult (unknown phase). In cartesian coordinates, the convolution kernels for EELS and SNOM obtained from Eqs. (63) and (72) read

$$\begin{aligned} B^{\text{eels}}(x,y,z) &= e^{i\frac{\omega}{v}z}K_0\left(\frac{\omega}{v}\sqrt{x^2+y^2}\right),\\ B^{\text{snom}}(x,y,z) &= \frac{z}{(x^2+y^2+z^2)^{3/2}}. \end{aligned} \qquad (73)$$

Note that in SNOM, the singularity already discussed above (see Secs. VI and IX) is not involved in the previous calculations because we have considered a dipole-probe either outside or inside the particle. However, it is possible to take the limit $\boldsymbol{r}\to\boldsymbol{s}$ in the final expressions for a given geometry. By using the modal expansions derived in this paper, we get (calculations not shown here) a divergence in $1/z^3$ in the case of a semi-infinite plane (dipole-probe infinitely close to the surface) and a divergence at the boundary of a spherical particle of radius R when $\boldsymbol{r}\to R$.

XI. DISCUSSION OF EELS/SNOM

We are now in the position to discuss the link between the experimental signals obtained by EELS and SNOM and the eigencharge densities $\sigma^i(\boldsymbol{s})$ of the system studied. It is now well-known that the quantity measured in EELS or SNOM experiments is related to the electromagnetic local density of states (EMLDOS) of the particle.[14,29] In the case where the excitations are photons, the EMLDOS has an unique modal decomposition and the interpretation of this quantity in terms of the spatial distribution of photonic mode is easy. In the case of surface excitations in the nonretarded approximation, for which no modal decomposition in terms of modes were available before the present work, the things are a little harder. Indeed, it appears that three different modal decompositions can be used equivalently but with a different physical interpretation. Despite these differences, the energy position of the maxima of these three expressions, both in EELS and SNOM, is given by that of $\Im[-g_i(\omega)]$. However, the expressions (58) and (66) for EELS seem to suggest that EELS is a good measure of the eigenpotential or the electric eigenfield squared along z due to $\sigma^i(\boldsymbol{s})$, but nevertheless evaluated in the momentum space along the direction of propagation of the incident electrons. Similarly, the expression (69) for SNOM suggests that the SNOM is a good measure of the electric field squared along z evaluated in the real space. In addition, the EELS and the SNOM can be directly related to the eigencharge density through a convolution [see Eqs. (63) and (72)]. All these equivalent descriptions have to be confronted to the problems of interpretation reported on whether the EELS is a good measure of the z-EMLDOS or the potential in full real space.[43]

The relation between these three expressions is more intuitive in the particular case of a thin nanoparticle for which the symmetry plane is perpendicular to z (such as that shown in Fig. 2). Note that this type of nanoparticles is widespread in nanoplasmonics and have been widely studied by EELS[3,36] or by other means.[44] Moreover, the most surprising experimental results are obtained with these structures, for which the symmetry is particularly well adapted to the geometry of the experiment. In these nanoparticles, the symmetry arguments lead directly to the existence of two families of modes: those at low energy are symmetric in charge with respect to the horizontal plane of symmetry of the structure (S modes) and those at high energy are antisymmetric (A modes). We see in Fig. 2 that both modes S and A modes are associated with the creation of a standing wave for the charge density (plasmonic standing wave). In the case of a thin nanoparticle, $s^{\parallel}\ll v\omega$. Thus, the exponential term in Eq. (63) equals 1. This makes more intuitive the expression (63): we directly see that an EELS image filtered at a given energy is given by the square of the eigencharge density (which is now a 2D function) convoluted to a Coulombic kernel. As expected from previous works on the inelastic delocalization, the smaller the electron speed, the smaller the effect of the convolution. In other words, the delocalization of the inelastic signal, due to the Coulombic interaction, is interpreted here as a convolution of the eigencharge density, by the Coulombic kernel, mode per mode.

It is necessary now to make a few remarks. First, because of the energy dependence of the convolution kernel, it is different for each mode. Practically, this means that we can not quantitatively compare the spatial distribution of the charge density in the x-y plane of the particle for two different modes if there was no estimates *a priori* of the different convolution kernels of these two modes. Second, the maxima observed in the EELS filtered images can be shifted relative to those

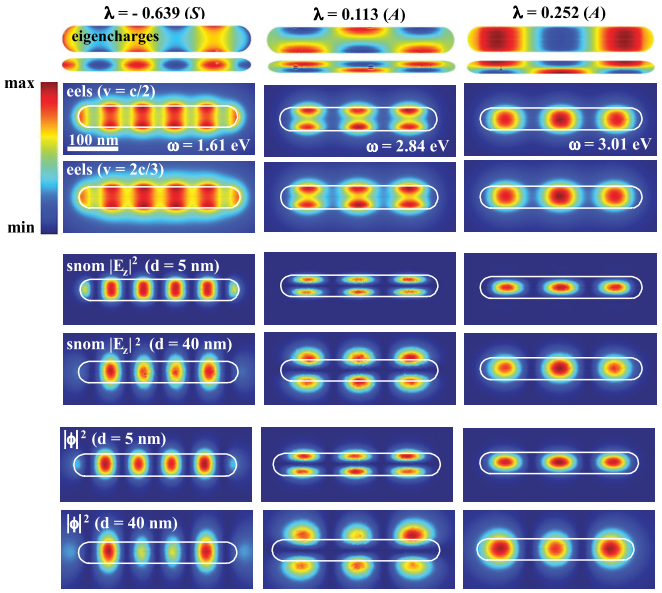

FIG. 2. (Color online) Electromagnetic signals obtained from BEM calculations for a thin particle in silver embedded in vacuum (aspect ratio = 15) for a symmetric eigenmode (first column) and two antisymmetric eigenmodes (second and third columns). The first row gives the spatial distribution of the geometric eigencharges (the face and the side are represented) (color scale: min $<$ 0 and max $>$ 0). The second and third rows give the EELS signal, respectively for electrons traveling with velocity $v = c/2$ and $2c/3$ (scale bar: min = 0). The fourth and fifth rows give the SNOM signal, respectively for a probe at $d = 5$ and 40 nm above the particle (scale bar: min = 0). The sixth and seventh rows give the potential squared, respectively at $d = 5$ and 40 nm above the particle (scale bar: min = 0). For each mode, the energy was calculated using the relation $\omega_i = \omega_p/\sqrt{2}\sqrt{1+\lambda_i}$ for a nonlossy Drude's model. The intensity ratio is (by increasing of energy) for EELS ($v = c/2$: 1|0.8|1 and $v = 2c/3$: 1|0.8|1.1) for SNOM ($d = 5$ nm: 1|0.3|0.8 and $d = 40$ nm: 1|0.03|1).

of the eigencharge densities, as observed experimentally and numerically in curved flat systems.[33] Indeed, the presence of the modulus squared in the expression (63) affects the convoluted charge densities, leading to nontrivial interferences between different parts of the spatial distribution of the charge densities and involves a nontrivial spatial distribution of the EELS signal (idem for SNOM). Here, we see the limits on the ability to compare directly the EELS or SNOM signal to the spatial distribution of the eigencharge densities rather than eigenpotential or electric eigenfield. In particular, the presence of the modulus squared after convolution implies that it is very difficult to extract the charge density from the EELS maps (or SNOM) by a deconvolution process since the kernel is very difficult to determine and for which a phasing issue will appear. Nevertheless, as shown in Fig. 2, SNOM and less trivially EELS give an image that is quite close to the spatial distribution of the eigencharge density at the surface of the particle, whatever the symmetry of the modes. In the case of nonflat nanoparticles, the convolution is less straightforward due to a mismatch between the experimental geometry and the symmetry of the particle.

It has been reported in Refs. 40 and 43 that we can find a plane above the particle in which the spatial distribution of the z-EMLDOS filtered at the energy of the mode i ($\propto |E_z^i(x,y,z)|^2$) or potential $|\phi^i(x,y,z)|^2$ mimics the spatial distribution of the EELS signal. This observation arises despite the fact that EELS is a measure of the electric field along z squared $[|E_z^i(x,y,q)|^2]$ or potential $[|\phi^i(x,y,q)|^2]$ in the momentum space along z. The present formalism helps in interpreting these facts, surprising at first sight, in the case of a flat nanoparticle. In the nonretarded approximation, the potential is a symmetric and monotone function in z on each side of the plane. The spatial extension along z is roughly a decreasing exponential with a decay length of the order of the wavelength of excitation in the plane of the particle, which depends on the order of the mode: $\phi^i(x,y,z) \sim \Phi^i(x,y)e^{-k^i z}$. The gradient along z of the potential [i.e., $E_z^i(x,y,z)$] or its Fourier transform along z [i.e., $\phi^i(x,y,q) \sim E_z^i(x,y,q)$] give functions with the same spatial distribution in the plane of the particle, given by $\Phi^i(x,y)$ (which provides also information on the physics of the underlying plasmons) and the same exponential decrease along z. Therefore, for flat particles, the EELS signal (or SNOM) is similar to the spatial distribution in a plane above the particle (provided that $z \neq 0$ since in this case the electric field is zero for S modes, while the potential is not null) both the potential or the electric field along z (or z-EMLDOS) so that in this case, the Fourier transform is in fact irrelevant (see Fig. 2).

XII. DISCUSSION OF THE SPATIAL COHERENCE

Here, we discuss the loss of spatial coherence of the modes defined by Eq. (8). This equation gives a set of geometric eigenmodes $\sigma^i(\boldsymbol{s})$, each with an eigenvalue λ_i defined perfectly whatever the nature of the media constituting the particle and its environment—dissipative or not. As an example, Fig. 3(a) shows the spatial distribution of consecutive eigenmodes of a nanoantenna. These spatial distributions are completely independent of the media constituting the particle and its environment but depend only on the geometry of the particle. This means that for structures having the same shape, both the λ_i and $\sigma^i(\boldsymbol{s})$ will be identical whatever the type of the excitations (interband transitions, excitons, plasmons, etc.) and the nature of the media (dissipative or not). This seems to be in contradiction with the experiments for which it is expected that the spatial distributions are well defined for surface plasmons only in metals and not in bad metals or insulators. In other words, this contradicts the common experience in which the experimental results depend on the medium studied and not only on its geometry. This apparent contradiction is due to the fact that in an experiment, this is not directly the material independent eigencharges densities that are measured. This is rather a quantity close to the EMLDOS of the object of interest filtered around a given energy.

The Sec. VI showed that we can express the EMLDOS in the form of a modal decomposition in terms of electric fields due to the geometric eigenmodes $\sigma^i(\boldsymbol{s})$ (idem for EELS and SNOM). For a given energy, the weight of each eigenmode i is given by $\Im[-g_i(\omega)]$ [see Fig. 3(b)]. The response function $g_i(\omega)$ depends on the energy through the dielectric functions of the media constituting the particle, its environment and the mode index. For a given material (having a given dielectric function) and at a given energy, if

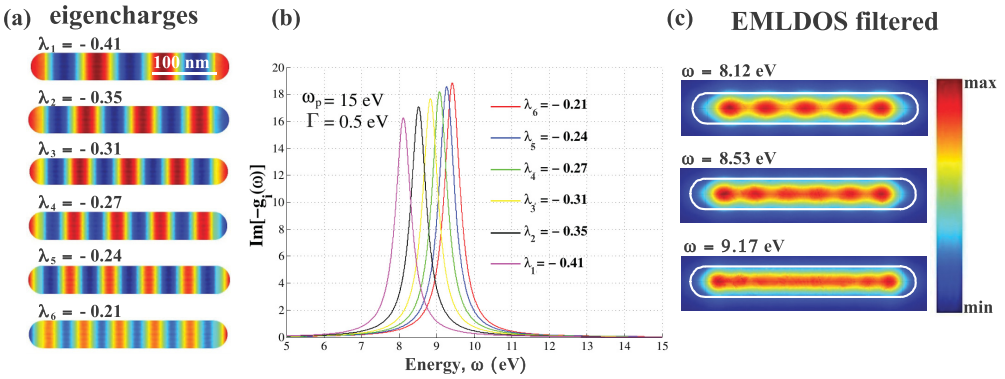

FIG. 3. (Color online) (a) BEM calculations of consecutive geometric eigencharges for a nanoantenna. (b) Graphic representation of the weights $\Im[-g_i(\omega)]$ involved in the expression (30) of the EMLDOS for each eigenmode. The nanoantenna is embedded in vacuum and it is described by a dissipative Drude's model: $\epsilon_1(\omega) = 1 - \omega_p^2/\omega(\omega + i\Gamma)$. (c) BEM calculations of the EMLDOS ($\mathrm{Tr}[\overleftrightarrow{\rho}^{\mathrm{SP}}(\boldsymbol{r},\omega)]$) filtered around a given energy at 30 nm above the particle. Color scale: for the eigencharges: min < 0 and max > 0 and for the EMLDOS: min, max > 0.

the weight of the geometric eigenmode i dominates over the weights of the others modes $(i-1, i+1, \ldots)$ in the modal decomposition, then the spatial distribution of the mode i will be clearly identified in the energy filtered EMLDOS. On the contrary, within the experimental resolution, if two or more modes overlap (i.e., in the case where several modes are excited with similar weights), the corresponding spatial distributions add incoherently in the EMLDOS involving a loss of spatial coherence (i.e., a jamming of the EMLDOS) [see Fig. 3(c)]. It is therefore the dispersion relations in the dielectric functions determining the evolution of $\Im[-g_i(\omega)]$, $\forall i$ (amplitude, FWHM, distance between the maxima), which will cause in experiments a difference between different types of studied materials. Obviously, the loss of temporal coherence due to the dissipation in the materials (increasing of the width of $\Im[-g_i(\omega)]$), induces an overlap of several modes at the same energy and consequently a loss of spatial coherence. However, a perhaps more subtle effect has to be noted: even for a (ideal) nondissipative metallic material, all ω_i (where $\lambda[\epsilon(\omega_i)] = \lambda_i$) tend to the same energy (the energy of the flat surface plasmon at the interface between two semi-infinite media, corresponding to $\lambda_i = 0$) when i tends to infinity. Near this limit, the density of states diverges (the dispersion curve of the excitation becomes horizontal), so even with a very good but necessarily finite experimental resolution, the loss of spatial coherence will always appear at large i.

Finally, in the case of a more complex material, it is remarkable to note that to the same eigenvalue λ_i may be associated different energies ω_i or even an energy continuum. This is because $\Im[-g_i(\omega)]$ can have several energy maxima. In the simplified case of a particle made up of a material described by a Drude-Lorentz model taking into account the presence of one interband transition, to each λ_i correspond two energy peaks. The ones corresponding to the interband transition are essentially due to maxima in the numerator of $\Im[-g_i(\omega)]$, which are almost independent of i. Thus it is remarkable that these secondary energy peaks, do not disperse much and pile up around $\omega = 2.5$ eV. Strikingly, the peaks due to a minimum of the denominator of $\Im[-g_i(\omega)]$ are strongly dependent on i and exhibit the dispersion behavior expected for surface plasmons [see Fig. 4(b)].

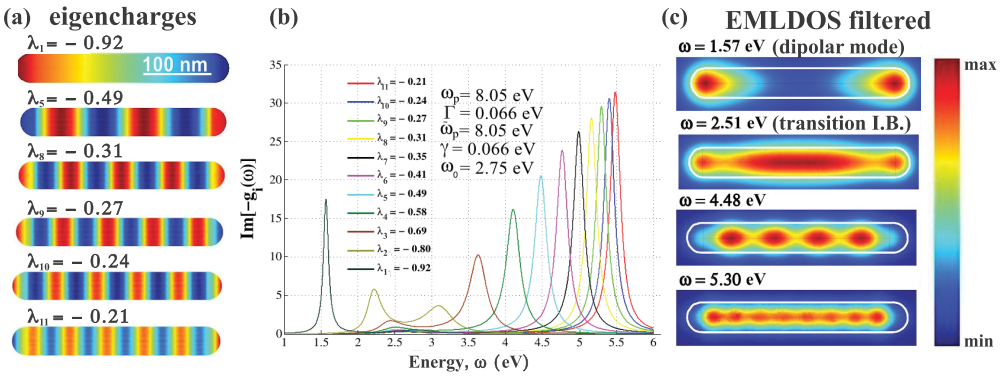

FIG. 4. (Color online) (a) BEM calculations of consecutive geometric eigencharges for a nanoantenna. (b) Graphic representation of the weights $\Im[-g_i(\omega)]$ involved in the expression (30) of the EMLDOS for each eigenmode. The nanoantenna is embedded in vacuum and it is described by a dissipative Drude-Lorentz model (including one interband transition): $\epsilon_1(\omega) = 1 - \omega_p^2/\omega(\omega + i\Gamma) + \tilde{\omega}_p^2/[(\omega_0^2 - \omega^2) - i\gamma\omega]$.[45] (c) BEM calculations of the EMLDOS ($\mathrm{Tr}[\overleftrightarrow{\rho}^{\mathrm{SP}}(\boldsymbol{r},\omega)]$) filtered around a given energy at 30 nm above the particle. (Color scale) for the eigencharges: min < 0 and max > 0 and for the EMLDOS: min, max > 0.

The loss of spatial coherence appears again at high energy but also more importantly around $\omega = 2.5$ eV [see Fig. 4(c)]. Such effects have already been observed experimentally in nanocylinders[9,46] and discussed theoretically in this highly symmetric case.[46,47]

XIII. CONCLUSIONS

We have derived an universal expression of the plasmonic EMLDOS including the dissipation and we showed that the expression obtained in the nondissipative limit is identical to that the EMLDOS well-known for photonic structures. Various equivalent modal decompositions of the scalar Green's function for the potential and the dyadic Green's tensor for the electric field have been obtained in terms of the geometric eigenmodes, which allowed us to obtain various expressions for EELS and SNOM. These expressions allowed us to show that energy filtered EELS and SNOM signals are a measure of the eigencharge density at the boundary of the particle but convoluted by a kernel having as the origin the Coulombic interaction. Also, EELS is a measure of the eigenpotential or the eigenelectric field in the momentum space along the direction of the incident electrons and SNOM is a measure of the eigenelectric field in real space. The particular case of a flat nanoparticle has been studied. A new type of LDOS, called *geometric local density of states* or GLDOS, defined in the complex plane has been introduced by analogy with the EMLDOS defined in the real space subtended by the energy. It has been shown that the GLDOS is independent of the energy and the nature of the media but depends only on the geometry of the particle. Finally, we showed that the energy dispersion of the dielectric functions of the underlying media is responsible for a loss of spatial coherence of the geometric eigenmodes.

Some other applications of our formalism can now be considered as the calculation of the localization radius of the eigenmodes defined from the statistical moment of order one and two of the electric field squared, which are well-known quantities in disordered nanosystems.[27] Also, another application concerns the calculation of the quasistatic creation and annihilation surface plasmon operators that appear in quantum plasmonics including the dissipative phenomena. Finally, an extension of our formalism for the retarded case would be worth to consider, as many nanooptical phenomena are not purely quasistatic and marked differences between relativistic modes and quasistatic ones may be found.[48]

ACKNOWLEDGMENTS

The authors acknowledge financial support from the European Union under the Framework 6 program under a contract for an Integrated Infrastructure Initiative. Reference 026019 ESTEEM. Also, we thank G. C des Francs for help with SNOM expressions.

APPENDIX A: PROPERTIES OF NORMALIZATION OF THE ELECTRIC FIELDS

Let Ω_1 and $\partial\Omega_1$ the volume and the boundary of the particle respectively and let Ω_2 the volume occupied by the environment of the particle. From now, in order to simplify the calculations, we will forget the notation "bound" used up to now for the potential and the electric field.

We have successively:

$$\begin{aligned}
&\oint_{\partial\Omega_1} ds\phi^i(\boldsymbol{s})^*\boldsymbol{n}\cdot\nabla\phi^j(\boldsymbol{s})\\
&= \oint_{\partial\Omega_1} ds \oint_{\partial\Omega_1} ds' \frac{\sigma^i(\boldsymbol{s}')^*}{|\boldsymbol{s}-\boldsymbol{s}'|}\oint_{\partial\Omega_1} ds'' F(\boldsymbol{s},\boldsymbol{s}'')\sigma^j(\boldsymbol{s}'')\\
&= \oint_{\partial\Omega_1} ds \oint_{\partial\Omega_1} ds'\sigma^i(\boldsymbol{s}')^*\\
&\quad\times\oint_{\partial\Omega_1} ds''\sigma^j(\boldsymbol{s}'')\frac{[F(\boldsymbol{s},\boldsymbol{s}')-2\pi\delta(\boldsymbol{s}-\boldsymbol{s}')]}{|\boldsymbol{s}-\boldsymbol{s}''|}\\
&= \oint_{\partial\Omega_1} ds \oint_{\partial\Omega_1} ds'\sigma^i(\boldsymbol{s}')^*\oint_{\partial\Omega_1} ds''\sigma^j(\boldsymbol{s}'')\frac{F(\boldsymbol{s},\boldsymbol{s}')}{|\boldsymbol{s}-\boldsymbol{s}''|}\\
&\quad-2\pi\oint_{\partial\Omega_1} ds\sigma^i(\boldsymbol{s})^*\oint_{\partial\Omega_1} ds''\frac{\sigma^j(\boldsymbol{s}'')}{|\boldsymbol{s}-\boldsymbol{s}''|}. \qquad \text{(A1)}
\end{aligned}$$

By using Eq. (8) and the orthogonality property (9) between the $\sigma^i(\boldsymbol{s})$, we obtain easily from Eq. (A1) the relation

$$\oint_{\partial\Omega_1} ds\phi^i(\boldsymbol{s})^*\boldsymbol{n}\cdot\nabla\phi^j(\boldsymbol{s}) = -2\pi(1-\lambda_i)\delta_{ij}. \qquad \text{(A2)}$$

By using now the divergence theorem[30] and the fact that $\nabla^2\phi^i = 0$ (free oscillations) and $\boldsymbol{E}^i = -\nabla\phi^i$, the previous boundary integral becomes a volume integral:

$$\int_{\Omega_1} d\boldsymbol{r}\boldsymbol{E}^i(\boldsymbol{r})^*\cdot\boldsymbol{E}^j(\boldsymbol{r}) = 2\pi(1-\lambda_i)\delta_{ij}. \qquad \text{(A3)}$$

By using a similar demonstration outside the particle, we obtain

$$\int_{\Omega_2} d\boldsymbol{r}\boldsymbol{E}^i(\boldsymbol{r})^*\cdot\boldsymbol{E}^j(\boldsymbol{r}) = 2\pi(1+\lambda_i)\delta_{ij}. \qquad \text{(A4)}$$

When $i \neq j$, Eqs. (A3) and (A4) show that the electric fields $\boldsymbol{E}^i(\boldsymbol{r})$ and $\boldsymbol{E}^j(\boldsymbol{r})$ are separately orthogonal inside and outside the particle. This result has already been reported in Ref. 24. When $i = j$, Eqs. (A3) and (A4) give the normalization of the electric field in each region:

$$\int_{\Omega_1} d\boldsymbol{r}|\boldsymbol{E}^i(\boldsymbol{r})|^2 = 2\pi(1-\lambda_i) \qquad \text{(A5)}$$

and

$$\int_{\Omega_2} d\boldsymbol{r}|\boldsymbol{E}^i(\boldsymbol{r})|^2 = 2\pi(1+\lambda_i) \qquad \text{(A6)}$$

then finally,

$$\int_{\Omega_1} d\boldsymbol{r}|\boldsymbol{E}^i(\boldsymbol{r})|^2 + \int_{\Omega_2} d\boldsymbol{r}|\boldsymbol{E}^i(\boldsymbol{r})|^2 = 4\pi. \qquad \text{(A7)}$$

Note that the normalization property (A7) depends on the orthogonality property between the eigencharges [see Eq. (9)]. It is quite possible to multiply the eigencharges by a constant so that the delta function which appears in Eq. (9) is scaled by a constant (i.e., $\delta_{ij} \to \delta_{ij}/a$).[25] Obviously, this constant can be chosen so that the normalization of the electric field gives the unity instead of 4π.

APPENDIX B: INTEGRATION OF $\Im[-g_i(\omega)]$

The integrations over ω, which appear in Eqs. (37)–(39), can be performed by using the first Kramers-Kronig's relation.[32] Let us consider a complex function of real variable $\omega > 0$: $f(\omega) = f'(\omega) + if''(\omega)$. If f verifies the following properties: (1) the integral of $f(\omega)/\omega$ along an infinite semicircle located in the upper half of the complex plane tends to 0. For this, it is sufficient that $f(\omega) \to 0$ when $\omega \to \infty$ and (2) the real part of f is even and its imaginary part is odd with respect to ω, then f satisfies the first Kramers-Kronig's relation (K-K),

$$f'(\omega) = \frac{2}{\pi}\mathcal{P}\int_0^{+\infty} d\Omega \frac{\Omega f''(\Omega)}{\Omega^2 - \omega^2}. \tag{B1}$$

If $f''(\omega)$ has no singularities for $\omega = 0$, we can pass to the limit $\omega \to 0$ in Eq. (B1) and write

$$f'(\omega = 0) = \frac{2}{\pi}\int_0^{+\infty} d\Omega \frac{f''(\Omega)}{\Omega}. \tag{B2}$$

For dielectric functions physically acceptable, i.e., for which

$$\begin{cases} \epsilon'_{1,2}(\omega = 0) \sim 1 & \text{(finite real part at } \omega = 0\text{)}, \\ \epsilon'_{1,2}(-\omega) = \epsilon'_{1,2}(\omega) & \text{(even function)}, \\ \epsilon_{1,2}(\omega) \to 1 & \text{when} \quad \omega \to \infty, \end{cases} \tag{B3}$$

and

$$\begin{cases} \epsilon''_{1,2}(\omega = 0) \sim 1/\omega^n, & n > 0, \\ \epsilon''_{1,2}(-\omega) = -\epsilon''_{1,2}(\omega) & \text{(odd function)}, \end{cases} \tag{B4}$$

the function $\Im[-g_i(\omega)]$ is an odd function of ω, which has no singularities for $\omega = 0$ and more, the function $\Re[-g_i(\omega)]$ is an even function of ω. Now, assuming that $\epsilon_{1,2}(\omega) \to 1$ when $\omega \to \infty$, the function

$$-g_i(\omega) = \frac{-2}{\epsilon_1(\omega)(1+\lambda_i) + \epsilon_2(\omega)(1-\lambda_i)} \tag{B5}$$

tends to -1 when $\omega \to \infty$ and thus (B2) is not applicable to $[-g_i(\omega)]$. However, we can apply it to $[-g_i(\omega) + 1]$, which verifies all the conditions to use K-K and thus

$$\int_0^{+\infty} \frac{d\omega}{\omega}\Im[-g_i(\omega)] = \frac{\pi}{2}\{\Re[-g_i(\omega = 0)] + 1\}. \tag{B6}$$

Under the assumptions (B3) and (B4), we get easily that $\Re[g_i(\omega = 0)] = 0$ and finally,

$$\int_0^{+\infty} \frac{d\omega}{\omega}\Im[-g_i(\omega)] = \frac{\pi}{2}. \tag{B7}$$

By a similar reasoning, we obtain the others integrals well-known in literature:

$$\int_0^{+\infty} \frac{d\omega}{\omega}\Im\left[-\frac{1}{\epsilon_1(\omega)}\right] = \int_0^{+\infty} \frac{d\omega}{\omega}\Im\left[-\frac{1}{\epsilon_2(\omega)}\right] = \frac{\pi}{2}. \tag{B8}$$

*kociak@lps.u-psud.fr

[1] I. Friedler, C. Sauvan, J. Hugonin, P. Lalanne, J. Claudon, and J. Gérard, Opt. Express **17**, 2095 (2009).
[2] D. Rossouw, M. Couillard, J. Vickery, E. Kumacheva, and G. Botton, Nano Lett. **11**, 1499 (2011).
[3] J. Nelayah, M. Kociak, O. Stéphan, F. J. García de Abajo, M. Tenc, L. Henrard, D. Taverna, I. Pastoriza-Santos, L. M. Liz-Marzan, and C. Colliex, Nat. Phys. **3**, 348 (2007).
[4] S. Empedocles and M. Bawendi, Science **278**, 2114 (1997).
[5] K. Imura and H. Okamoto, Bull. Chem. Soc. Jpn. **81**, 659 (2008).
[6] Y. De Wilde, F. Formanek, R. Carminati, B. Gralak, P. A. Lemoine, K. Joulain, J. P. Mulet, Y. Chen, and J. J. Greffet, Nature (London) **444**, 740 (2006).
[7] N. Yamamoto, K. Araya, and F. J. García de Abajo, Phys. Rev. B **6420**, 205419 (2001).
[8] L. F. Zagonel *et al.* , Nano Lett. **11**, 568 (2011).
[9] R. Arenal, O. Stephan, M. Kociak, D. Taverna, A. Loiseau, and C. Colliex, Phys. Rev. Lett. **95**, 127601 (2005).
[10] M. Bosman, V. J. Keast, M. Watanabe, A. I. Maaroof, and M. B. Cortie, Nanotechnology **18**, 165505 (2007).
[11] L. Douillard, F. Charra, Z. Korczak, R. Bachelot, S. Kostcheev, G. Lerondel, P. M. Adam, and P. Royer, Nano Lett. **8**, 935 (2008).
[12] A. Dereux, C. Girard, and J. C. Weeber, J. Chem. Phys. **112**, 7775 (2000).
[13] K. Joulain, R. Carminati, J. P. Mulet, and J. J. Greffet, Phys. Rev. B **68**, 245405 (2003).
[14] F. J. García de Abajo and M. Kociak, Phys. Rev. Lett. **100**, 106804 (2008).
[15] G. C. des Francs, C. Girard, J. C. Weeber, C. Chicane, T. David, A. Dereux, and D. Peyrade, Phys. Rev. Lett. **86**, 4950 (2001).
[16] F. Ouyang, P. E. Batson, and M. Isaacson, Phys. Rev. B **46**, 15421 (1992).
[17] F. J. García de Abajo and J. Aizpurua, Phys. Rev. B **56**, 15873 (1997).
[18] D. R. Fredkin and I. D. Mayergoyz, Phys. Rev. Lett. **91**, 253902 (2003).
[19] M. I. Stockman, S. V. Faleev, and D. J. Bergman, Phys. Rev. Lett. **88**, 067402 (2002).
[20] J. Aizpurua, A. Howie, and F. J. García de Abajo, Phys. Rev. B **60**, 11149 (1999).
[21] F. J. García de Abajo and A. Howie, Phys. Rev. B **65**, 115418 (2002).
[22] U. Hohenester and J. R. Krenn, Phys. Rev. B **72**, 195429 (2005).
[23] U. Hohenester, H. Ditlbacher, and J. R. Krenn, Phys. Rev. Lett. **103**, 106801 (2009).
[24] I. D. Mayergoyz, D. R. Fredkin, and Z. Zhang, Phys. Rev. B **72**, 155412 (2005).
[25] F. Ouyang and M. Isaacson, Philos. Mag. B **60**, 481 (1989).
[26] D. J. Bergman and M. I. Stockman, Phys. Rev. Lett. **90**, 027402 (2003).
[27] M. I. Stockman, S. V. Faleev, and D. J. Bergman, Phys. Rev. Lett. **87**, 167401 (2001).
[28] M. I. Stockman, D. J. Bergman, and T. Kobayashi, Phys. Rev. B **69**, 054202 (2004).
[29] G. C. des Francs, C. Girard, and A. Dereux, J. Chem. Phys. **117**, 4659 (2002).

[30]J. D. Jackson, *Classical Electrodynamics*, 2nd ed. (John Wiley & Sons, Inc., New York, 1975).
[31]C. A. Guerin, B. Gralak, and A. Tip, Phys. Rev. E **75**, 056601 (2007).
[32]L. D. Landau and E. M. Lifshitz, *Electrodynamics of Continuous Media* (Pergamon, Oxford, 1960).
[33]G. Boudarham, N. Feth, V. Myroshnychenko, S. Linden, J. García de Abajo, M. Wegener, and M. Kociak, Phys. Rev. Lett. **105**, 255501 (2010).
[34]L. Gu, W. Sigle, C. T. Koch, B. Ögüt, P. van Aken, N. Talebi, R. Vogelgesang, J. Mu, X. Wen, and J. Mao, Phys. Rev. B **83**, 195433 (2011).
[35]O. Nicoletti, M. Wubs, N. Mortensen, W. Sigle, P. van Aken, and P. Midgley, Opt. Express **19**, 15371 (2011).
[36]J. Nelayah, M. Kociak, O. Stéphan, N. Geuquet, L. Henrard, F. J. García de Abajo, I. Pastoriza-Santos, L. M. Liz-Marzán, and C. Colliex, Nano Lett. **10**, 902 (2010).
[37]M. W. Chu, V. Myroshnychenko, C. H. Chen, J. P. Deng, C. Y. Mou, and F. J. García de Abajo, Nano Lett. **9**, 399 (2009).
[38]M. N'Gom, S. Li, G. Schatz, R. Erni, A. Agarwal, N. Kotov, and T. B. Norris, Phys. Rev. B **80**, 113411 (2009).
[39]N. Zabala and A. Rivacoba, Phys. Rev. B **48**, 14534 (1993).
[40]F. J. García de Abajo and M. Kociak, Phys. Rev. Lett. **100**, 106804 (2008).
[41]J. J. Greffet and R. Carminati, Prog. Surf. Sci. **56**, 133 (1997).
[42]J. A. Porto, R. Carminati, and J. J. Greffet, J. Appl. Phys. **88**, 4845 (2000).
[43]U. Hohenester, H. Ditlbacher, and J. R. Krenn, Phys. Rev. Lett. **103**, 106801 (2009).
[44]M. Rang, A. C. Jones, F. Zhou, Z. Y. Li, B. J. Wiley, Y. N. Xia, and M. B. Raschke, Nano Lett. **8**, 3357 (2008).
[45]L. Novotny and B. Hecht, *Principles of Nano-optics* (Cambridge University Press, Cambridge, 2006).
[46]M. Kociak, O. Stéphan, L. Henrard, V. Charbois, A. Rothschild, R. Tenne, and C. Colliex, Phys. Rev. Lett. **87**, 075501 (2001).
[47]D. Taverna, M. Kociak, V. Charbois, and L. Henrard, Phys. Rev. B **66**, 235419 (2002).
[48]S. Mazzucco, N. Geuquet, J. Ye, O. Stéphan, W. Van Roy, P. Van Dorpe, L. Henrard, and M. Kociak, Nano Lett. **12**, 1288 (2012).